

Characterization and Modeling of Recycled Pavement Sections

FINAL REPORT
November 2017

Submitted by:

Wenjing Xue
Research Associate

Gerardo W. Flintsch
Director & Professor

Brian K. Diefenderfer
Associate Principal Research Scientist

Benjamin F. Bowers
Research Scientist

Center for Sustainable Transportation Infrastructure
Virginia Tech Transportation Institute
3500 Transportation Research Plaza
Blacksburg, VA, 24061

External Project Manager
Benjamin Bowers
Research Scientist
Virginia Center for Transportation Innovation and Research
530 Edgemont Road
Charlottesville, VA 22903

In cooperation with

Rutgers, The State University of New Jersey
And
Virginia Department of Transportation
And
U.S. Department of Transportation
Federal Highway Administration

Disclaimer Statement

The contents of this report reflect the views of the authors, who are responsible for the facts and the accuracy of the information presented herein. This document is disseminated under the sponsorship of the Department of Transportation, University Transportation Centers Program, in the interest of information exchange. The U.S. Government assumes no liability for the contents or use thereof.

The Center for Advanced Infrastructure and Transportation (CAIT) is a National UTC Consortium led by Rutgers, The State University. Members of the consortium are the University of Delaware, Utah State University, Columbia University, New Jersey Institute of Technology, Princeton University, University of Texas at El Paso, Virginia Polytechnic Institute, and University of South Florida. The Center is funded by the U.S. Department of Transportation.

1. Report No. CAIT-UTC-NC29		2. Government Accession No.		3. Recipient's Catalog No.	
4. Title and Subtitle Characterization and Modeling of Recycled Pavement Sections				5. Report Date December 2017	
				6. Performing Organization Code Virginia Tech/ CAIT	
7. Author(s) Wenjing Xue, Gerardo W. Flintsch, Brian K. Diefenderfer, Benjamin F. Bowers				8. Performing Organization Report No. CAIT-UTC-NC29	
9. Performing Organization Name and Address Center for Sustainable Transportation Infrastructure 3500 Transportation Research Plaza Blacksburg, VA 24061				10. Work Unit No.	
				11. Contract or Grant No. DTRT13-G-UTC28	
12. Sponsoring Agency Name and Address Center for Advanced Infrastructure and Transportation Rutgers, The State University of New Jersey 100 Brett Road Piscataway, NJ 08854				13. Type of Report and Period Covered Final Report 03/01/16 - 12/31/16	
				14. Sponsoring Agency Code	
15. Supplementary Notes U.S. Department of Transportation/OST-R 1200 New Jersey Avenue, SE Washington, DC 20590-0001					
16. Abstract <p>Because of its documented cost and environmental benefits, cold central plant recycling (CCPR) has attracted the interest of local and state departments of transportation. In 2015 two test pavement sections with CCPR as base layers were constructed at the Accelerated Pavement Testing facility located at the Virginia Tech Transportation Institute. The intention of this study is to investigate the effect of different overlays on CCPR material under accelerated loading. The two test sections (four test cells) had similar structures, but one lane was overlaid with a dense graded asphalt surface mixture of 76 mm (3 inches) while the other lane had only 38 mm (1.5 inches) of the same mixture. The CCPR base was 127 mm (5 inches) thick in both lanes.</p> <p>Pavement responses (longitudinal strain and vertical pressure) and vertical permanent deformation at the pavement surface were monitored throughout testing. The distribution of pressure versus depth showed that the thinner surface layer led to a steeper reduction of pressure in the surface and CCPR layers, which could produce increased rutting over time. Based on laser profiler measurements, rutting depth developed differently between the two lanes, as well as between the two test cells within the same lane. An empirical model was developed to compensate for the age effect in order to fairly evaluate the rutting performance of the different pavement sections. After being normalized by the model, the rut depth in the lane having the 76-mm (3-inch) surface layer was 62% of the rut depth in the lane having the 38-mm (1.5-inch) surface layer.</p>					
17. Key Words Cold Central Plant Recycling (CCPR), Accelerated Pavement Testing (APT), Heavy Vehicle Simulator (HVS), rutting, rutting model				18. Distribution Statement No restrictions	
19. Security Classification (of this report) Unclassified		20. Security Classification (of this page) Unclassified		21. No. of Pages Total # 20	22. Price

Table of Contents

Description of the Problem	1
Background	1
Problem Statement.....	2
Objective	2
Approach.....	2
Pavement Sections.....	2
Equipment.....	4
Experiment Timeline	5
Data Collection	6
Results.....	8
Dynamic Response	8
<i>Longitudinal Strain</i>	8
<i>Pressure</i>	9
Load Transfer.....	11
Rutting Depth	11
Discussion.....	15
Conclusions.....	15
References.....	16

List of Figures

FIGURE 1 Pavement sections layout and structures.....	3
FIGURE 2 Main equipment used in the APT program.....	4
FIGURE 3 Loading charts of the six test cells in lane 1 and lane 2.....	6
FIGURE 4 Pavement measurements.....	7
FIGURE 5 Strain fluctuations of cell 1B throughout the test.	8
FIGURE 6 Pressure vs. ESALs at different depths.	10
FIGURE 7 Load transferring in the pavement section.....	11
FIGURE 8 Rutting depth calculation demonstration.....	12
FIGURE 9 Rutting depths for the four test cells.	12
FIGURE 10 Comparison among the regression fitted results with rutting depth measurements.	14
FIGURE 11 Rutting depth predictions for 3-inch and 1.5-inch pavement sections.....	14

List of Tables

TABLE 1 Timeline of the APT on lane 1 and lane 2.....	5
---	---

DESCRIPTION OF THE PROBLEM

Background

Due to the growing volume of pavement material used around the world every year, finding ways to reduce paving costs and reduce their environmental impacts is crucial. Furthermore, the budget constraints faced by highway agencies can limit the amount of funding for a single project, which may in turn prevent the use of appropriate maintenance and rehabilitation strategies deep in the pavement structure. Fortunately, pavement recycling, specifically cold recycling, offers an economical solution to this issue.^[5] Pavement recycling techniques include hot in-place recycling, cold recycling, and full-depth reclamation (FDR). Cold recycling techniques, include cold in-place recycling (CIR) and cold central-plant recycling (CCPR), have attracted interest because of their documented cost and environmental benefits. A study by Liu et al. in 2014 [1] noted that using CCPR and CIR could reduce gas emissions significantly compared to hot mix asphalt (HMA). Cold recycling techniques have not commonly been used on primary roads in the United States because of the uncertainty of their long-term performance [2, 3].

Local and federal departments of transportation have initiated many research projects to explore the performance of various pavements resulting from these techniques. In 2011, the Virginia Department of Transportation (VDOT) [4] used FDR, CIR, and CCPR together in the rehabilitation of a 6 km (3.7 mi) two-lane section of southbound Interstate 81 in Augusta County, Virginia. Using specimens cored from the section, Apeageyi and Diefenderfer [4] conducted laboratory tests (gradation, binder content, density, indirect tensile strength, and resilient modulus) and found that recycled materials produced by CIR and CCPR have similar engineering properties. In 2016, Diefenderfer et al. [5] found that CCPR, CIR, and FDR recycling mixtures had a similar range of dynamic modulus values, and CCPR and CIR had a greater stiffness temperature dependency than that of FDR.

After observing promising results from the I-81 project, VDOT developed a companion study to optimize surfacing thickness on CCPR layers by sponsoring the construction of three test sections at the National Center for Asphalt Technology (NCAT) [6]. Each section featured a stone-matrix asphalt surface and Superpave dense-graded asphalt concrete layers above the CCPR layer. One study section had a total thickness of the asphalt layers of 152 mm (6 inches), and the other two sections had a total thickness of the asphalt layers of 102 mm (4 inches). All three sections had a CCPR thickness of 127 mm (5 inches). The test sections exhibited excellent performance under 10 million equivalent single axle loads (ESALs) over the initial 2-year test period [6]. The results from the NCAT study suggested that a 102-mm (4-inch) surface layer may be conservative, and the thickness of the surface layer could be further reduced to enhance cost effectiveness.

In 2015, VDOT initiated an Accelerated Pavement Testing (APT) program at Virginia Tech Transportation Institute (VTTI), employing a Heavy Vehicle Simulator (HVS) as its technological centerpiece. This program provides a testbed for pavements with varying structural and material compositions.

Problem Statement

Since the NCAT study suggest the possibility of further reducing the thickness of surface layer, two test lanes in the VTTI APT program were designed and constructed to explore the field performance of CCPR sections with different and thinner asphalt surfaces. Accelerated pavement tests need to be conducted to evaluate and compare the rutting resistance of the two structures.

OBJECTIVE

To characterize the field performance of CCPR sections placed at the VTTI APT facility, the following objectives were defined for this study:

- Understand the distribution of pavement dynamic responses (strain and pressure) within the CCPR test sections.
- Investigate the load transfer process(es) in different pavement structures.
- Evaluate the rutting performance of the CCPR sections under accelerated loading.
- Develop rut depth model for the CCPR test sections.

APPROACH

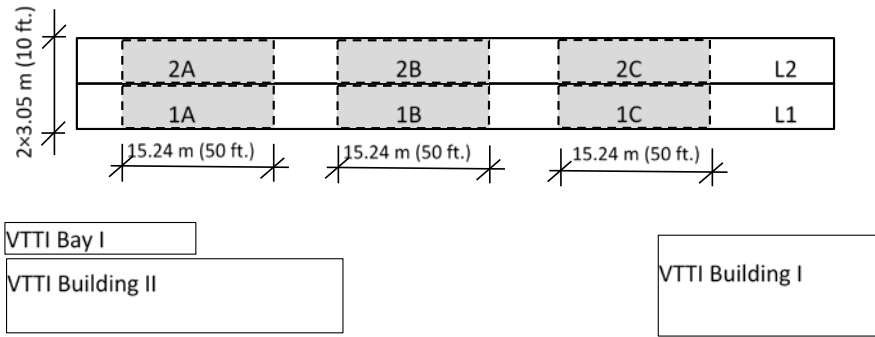
Pavement Sections

The APT facility at VTTI provides a testbed for pavements with varying structural and material compositions. Lanes 1 and 2 (L1 and L2 in FIGURE 1 (a)) are the two CCPR test lanes targeted in this study. These two lanes had similar structures, except that the surface layer in Lane 1 was 76 mm (3 inches) thick and the surface layer in Lane 2 was 38 mm (1.5 inches) thick. Each test lane is divided into three test cells: A, B and C. The whole structure lies on top of a foundation comprised of three 152-mm (6-inch) lifts of 21B aggregate between geogrid reinforcement.

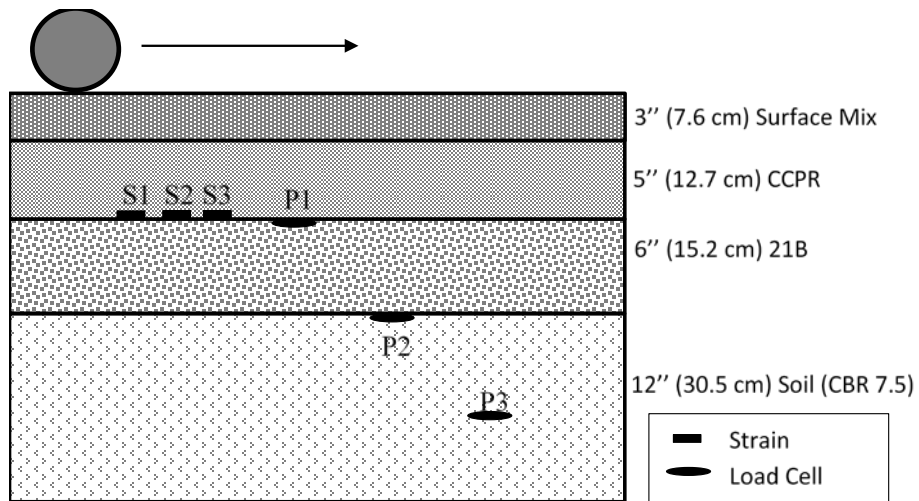
Both lanes feature a 127-mm (5-inch) CCPR base layer, a 203-mm (8-inch) 21B aggregate layer, and a 660-mm (26-inch) subgrade soil layer. The CCPR mix consists of reclaimed asphalt pavement (RAP), performance grade (PG) 64-22 bitumen, ordinary Portland cement, and water. Foaming water (2.3% by mass of bitumen) was injected into hot bitumen to produce foamed bitumen. The foamed bitumen (2.3% by mass of RAP) was added into RAP together with approximately 1.0% Portland cement (by mass of RAP) as the stabilizing agent. The material characterization of the CCPR mixture was performed on full-scale laboratory compacted specimens, which were in compliance with ASTM D6925-15. The dynamic modulus and the flow number tests were used to characterize the material.

Both lanes are overlaid with a 9.5-mm (nominal maximum aggregate size, NMAS) dense graded surface mix. The surface layer of lane 1 is 76 mm (3 inches) thick, as shown in FIGURE 1 (b), and lane 2's surface layer is 38 mm (1.5 inches) thick, as shown in FIGURE 1 (c). The surface mix was produced with 44% quartzite of size #8, 11% quartzite of size #10, 19% sand and 26% RAP (1/2 inch). PG 64-22 binder was used, and the content was 5.50%. The content of air voids (VTM) was 3.7%.

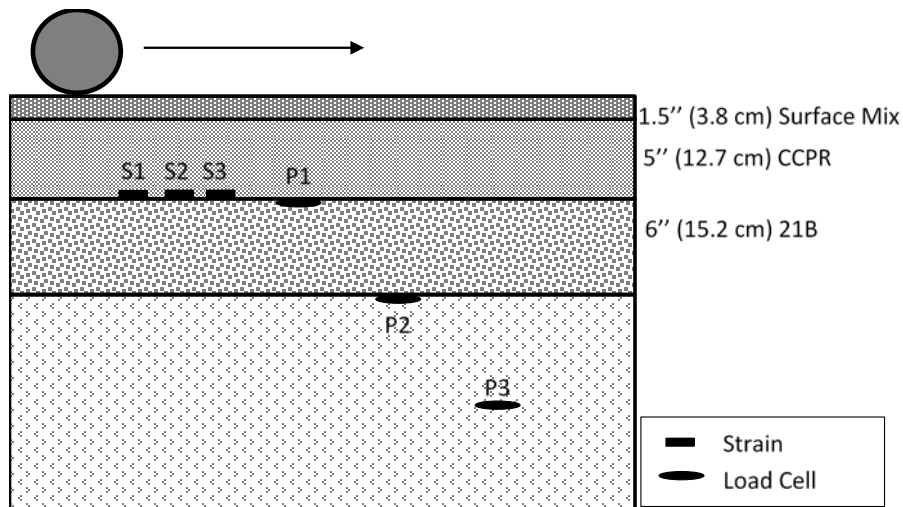
Cell B and C of each lane were instrumented with asphalt strain gauges, load cells, and thermocouples. All the strain gauges and load cells were installed on the centerline of the lane, and their locations are shown in FIGURE 1 (b) and (c).



(a) Layout



(b) Structure of lane 1 and instrumentation in cells 1B and 1C



(c) Structure of lane 2 and instrumentation in cells 2B and 2C

FIGURE 1 Pavement sections layout and structures.

Equipment

The main equipment used in the APT program includes the HVS, instruments to measure pavement or material response, and a data acquisition system (DAS).

By using an HVS, experiments can be conducted on pavement structures in a controlled manner that may not be possible in the field at no risk to the travelling public. The HVS used for all of the experimental loading, shown in FIGURE 2(a), was produced and acquired from Dynatest Consulting. This particular unit allows testing of sections at higher speeds and lengths. It is capable of testing at speeds up to 20 ± 3.2 km/h (12.4 ± 2 mph) with loads that range from approximately 26.7 to 100.1 kN (6 to 22.5 kips).

The instruments used in this study are asphalt strain gauges (Tokyo Sokki Kenkyujo Co. KM-100HAS), load cells (Geokon 3500), and thermocouples (Pyromation type T).



(a) HVS (Model MARK VI)



(b) Chassis with input modules and a controller



(c) Interaction interface

FIGURE 2 Main equipment used in the APT program.

The DAS is used to collect signals from all of the instruments and monitor pavement health status. Based on the instrumentation, corresponding input modules from National Instruments were installed in a chassis, as was a controller, as shown in FIGURE 2(b). An interactive interface was developed using the software LabVIEW, shown in FIGURE 2(c). Both the chassis and the interface device were housed in a weather-proof chamber (FIGURE 2(d)) located adjacent to the HVS.

Experiment Timeline

Accelerated pavement testing was conducted to evaluate the performance of the two CCPR pavement sections on each test cell. The test cells were tested under accelerated loading, with each subsequent test cell considered a replicate for its respective lane. In each test, the temperature of the surface layer was controlled at 40° C (104° F) as monitored by a thermocouple embedded at a depth of 5.1 cm (2 inches) from the pavement surface. The loading timeline and number of equivalent single axil loads (ESALs) applied to the pavement within the testing period is provided in TABLE 1.

TABLE 1 Timeline of the APT on lane 1 and lane 2

Cell	Period		Loading	
	Start	End	# of passes	# of ESALs
1A	10/20/2015	12/18/2015	62,167	294,790
1B	5/2/2016	7/11/2016	276,543	651,361
1C	7/25/2016	10/24/2016	267,029	588,717
2A	1/7/2016	2/4/2016	64,402	185,399
2B	2/19/2016	4/15/2016	229,496	336,592
2C	10/28/2016	12/23/2016	263,159	563,662

As TABLE 1 shows, cells 1A and 2A were not tested for the same duration as the other four cells. These two cells were not instrumented and were only used for refining the test methodology. As a result, only four test cells: 1B, 1C, 2B and 2C are discussed in detail henceforth.

During testing of each cell, the HVS was operating continuously with the exception of regular daily maintenance and occasional repairs. The wheel load was 40 kN (9 kips) during the first 6~7 weeks, 53.4 kN (12 kips) for one week, and to 66.7 kN (15 kips) for the following week to further accelerate the development of pavement distresses. After the wheel load was increased to 53.4 kN (12 kips) or 66.7 kN (15 kips), the HVS was still run at 40 kN (9 kips) for 15 minutes every morning after maintenance to capture pavement responses to at this load level throughout the entirety of the test. The loading charts of the six cells are summarized in FIGURE 3.

As shown in FIGURE 3, although the experimenter intended to load the four test cells in the same way, the actual loading history was actually not exactly the same. Cell 2B was the first tested, and it was discovered that some sensing devices weren't absolutely compatible with the DAS. Further, the experimental plan was undergoing adjustment. As a result, testing time for 2B was shorter than for the other three cells. Additionally, testing on 1C was forced to stop in middle for several weeks due to HVS repairs.

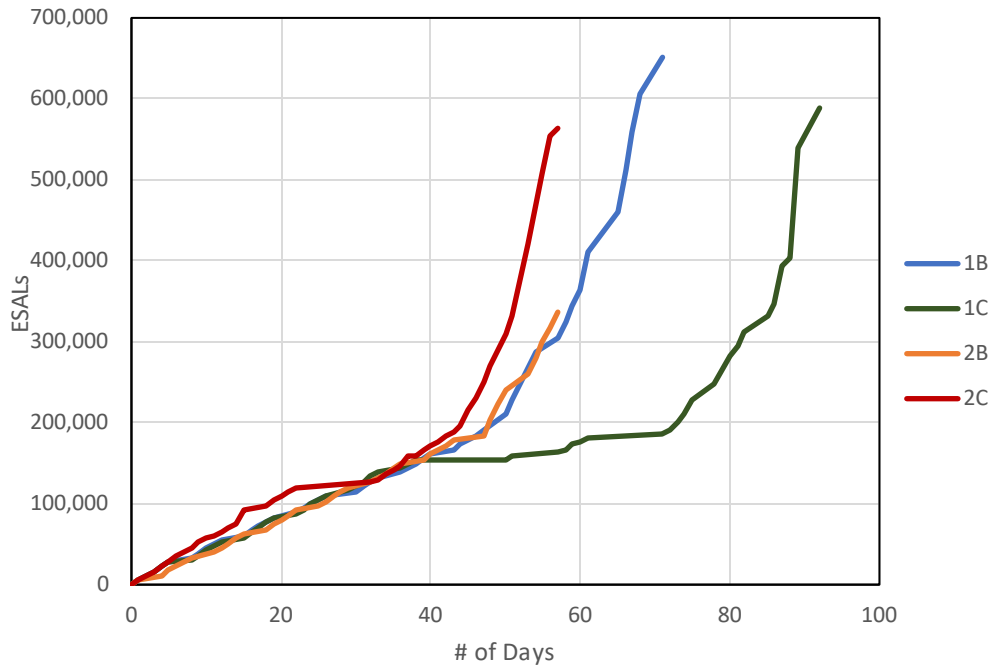


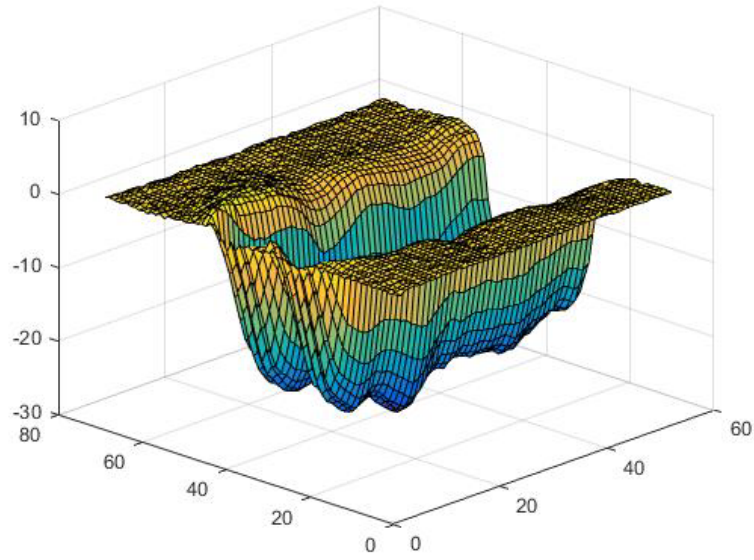
FIGURE 3 Loading charts of the six test cells in lane 1 and lane 2.

Data Collection

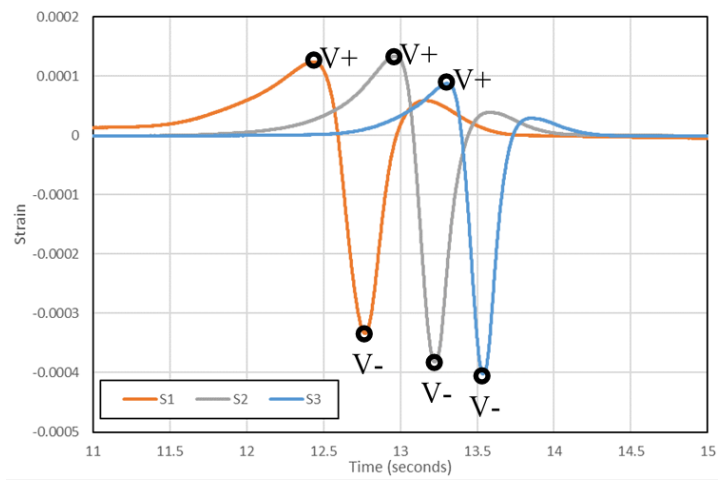
At the conclusion of the daily maintenance, procedure a profiler mounted on the carriage was used to scan the pavement surface to collect rutting measurements and generate a three-dimensional rutting plot. One scanned surface is shown in FIGURE 4 (a). While the HVS was applying repeated wheel loads on the test cell, the DAS collected the real-time pavement responses for 3 minutes every hour in the first week, and for 3 minutes every 3 hours in the following weeks. One signal segment of the strain gauges is shown in FIGURE 4 (b) and another of the load cells is shown in FIGURE 4 (c).

The daily rutting profile (FIGURE 4 [a]) was generated so that the rutting development curve could be developed over the duration of the test. The shape and magnitude of signals from the three strain gauges (FIGURE 4 (b)) are similar because they were all embedded on the center line with same depth and direction. Even so, there are slight variations in the magnitudes of strain. One possible reason for this is that the direction and location of the sensors may have changed slightly during the paving and compaction processes. The shape and magnitude of the fluctuations from the three load cells (FIGURE 4 [c]) illustrate the wheel load pressure transfer process within the pavement structure. The pressure decreases significantly as the depth increases.

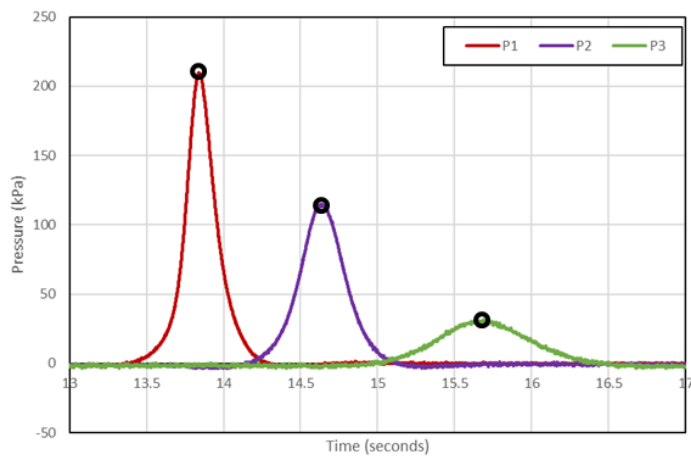
The peak points of each load cell signal fluctuation (FIGURE 4 [c]) were extracted and averaged for every 4-minute data segment (generally 16 or 17 passes) from the four test cells. The elastic strain fluctuation of pavement to wheel loads was represented by the difference between the maximum compressive strain (V+) and the maximum tensile strain (V-).



(a) Daily rutting surface (cell 1B, June 30, 2016)



(b) Real-time strain responses (June 30, 2016, 8:27 a.m.)



(c) Real-time load cell responses (June 30, 2016, 8:27 a.m.)

FIGURE 4 Pavement measurements.

RESULTS

Dynamic Response

Both pressure cell and strain gauge measure the dynamic pavement responses, which are sensitive to not only the current pavement modulus and loading profile, but also to the loading history and accumulative damage. As a result, it is not appropriate to compare pavement responses with different loading histories. In this experiment (as shown in FIGURE 3), cell 2B was tested first among the four, and its pressure signals were not collected with suitable DASs, so its final ESAL count is much smaller than the others. Testing for cell 1C was interrupted for more than 30 days because the HVS equipment was not operating properly. In this case, dynamic responses from cell 1C and 2B are not used in the analysis, and the responses from 1B and 2C will instead be used represent the two lanes in the analyses.

Longitudinal Strain

Because the three strain gauges were installed at the same location within the structure, their median measurements were used to increase reliability and reduce the effect of random factors when examining the strain fluctuation of the pavement under designed wheel loads. FIGURE 5 shows these strain fluctuations.

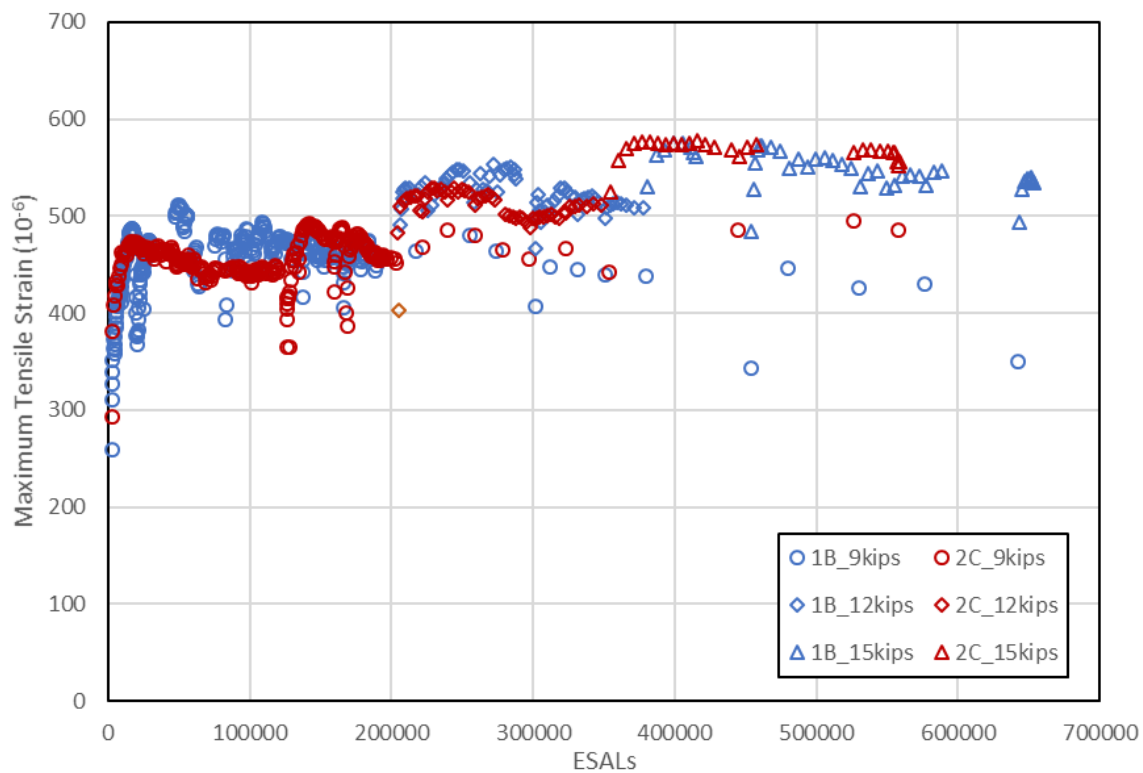


FIGURE 5 Strain fluctuations of cell 1B throughout the test.

As described previously, 53.4 kN (12 kips) and 66.7 kN (15 kips) were used to accelerate the development of rutting in the experiment. FIGURE 5 shows that strain response increased, but not linearly, when wheel load was increased.

The strain responses from 1B and 2C are compared in FIGURE 5 to reveal any potential difference between lane 1 and 2. The strain trends in the two lanes were close to each other; the strain in 1B was slightly higher before 350,000 ESALs, but lower in the latter half of the experiment.

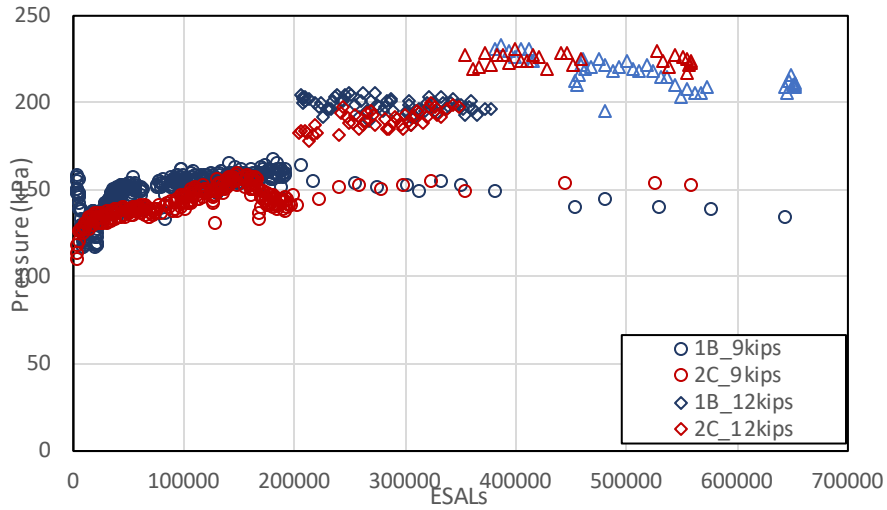
Since the strain presented in FIGURE 5 represents the elastic deformation of the pavement sections under the passing wheel loads, it can be used to evaluate the strength of the whole structure. In other words, lane 2 (38-mm [1.5-inch] surface layer) behaved similarly to lane 1 (76-mm [3-inch] surface layer) under wheel loads up to 350,000 ESALs, but the strength of its structure got smaller than lane 1 after that.

Pressure

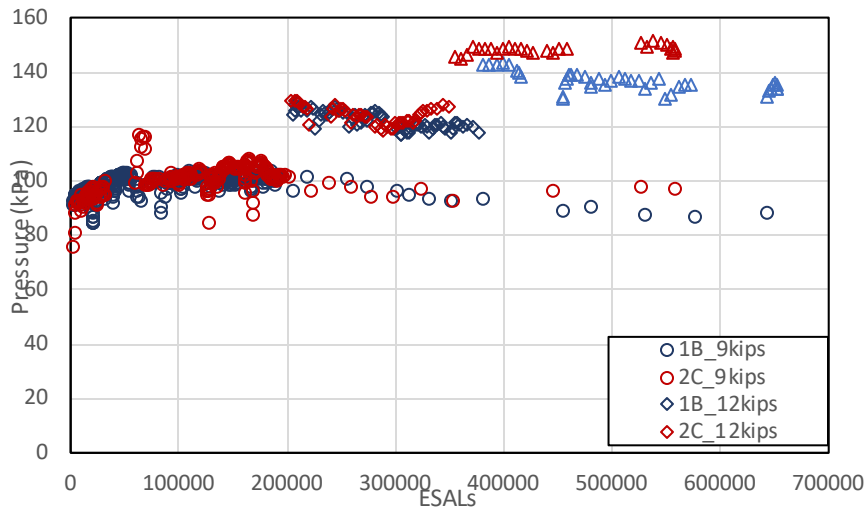
The pressure response from each testbed included three load levels (40, 53.4 and 66.7 kN [9, 12 and 15 kips]) and three locations (P1, P2, and P3). The pressure responses from cells 1B and 2C were compared at different depths in the pavement structure, as shown in FIGURE 6.

At the bottom of the CCPR base layer (FIGURE 6 [a]), the distribution of pressure changed frequently in the first stage because the layers were in the consolidation process, causing the aggregates and asphalt binder to move locally under the wheel load. The pressure measurements in 1B and 2C were similar in both trend and magnitude, even overlapping at points. At the bottom of the aggregate layer (FIGURE 6 [b]), the pressure measurements from 1B and 2C were close, overlapping before 300,000 ESALs. Beyond 300,000 ESALs, the pressure in 2C began to increase, becoming almost 10 kPa (1.45 psi) bigger than the pressure in 1B at 500,000 ESALs. In the middle of the subgrade (FIGURE 6 [c]), 2C's pressure readings were constantly higher than 2B's, with the difference increasing along with the number of ESALs. Readings from 1B and 2C both showed that the subgrade had consolidated prior to testing, and the readings stayed stable since the beginning.

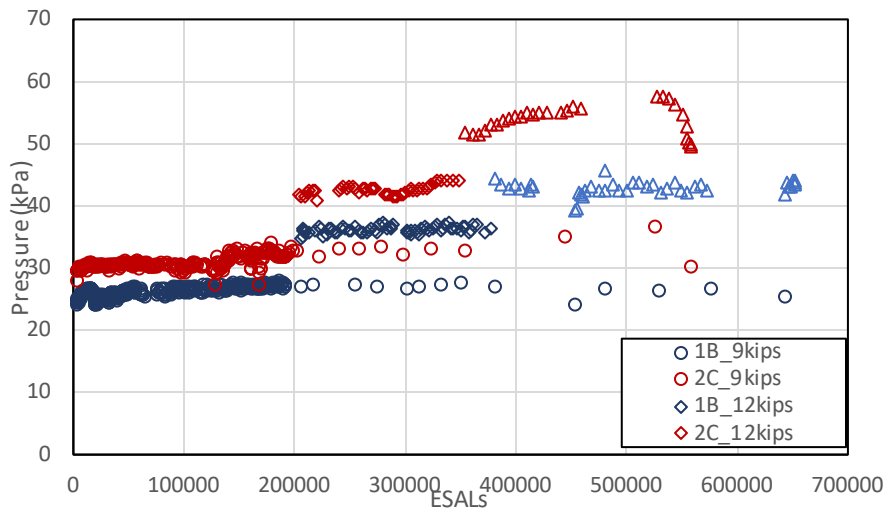
Specifically for FIGURE 6 (a), the pressure in test cell 2C changed dramatically during the consolidation process and became smaller than that of test cell 1B for pressure cell P1. One possible reason for this is that, during the process, 1B's thicker surface layer accommodated more local rearrangement of materials and induced higher pressure distribution. After the section became stable, the pressure measurements in test cell 2C were slightly larger than in test cell 1B. This is because lane 2's surface layer was thinner than lane 1's, and thus in lane 2 the identical wheel load was transferred to a smaller area than in lane 1.



(a) Pressure responses at bottom of the base layer (P1)



(b) Pressure responses at the bottom of the aggregate layer (P2)



(c) Pressure response at the middle of the subgrade layer (P3)

FIGURE 6 Pressure vs. ESALS at different depths.

Load Transfer

Pavement structures are designed to include multiple layers so that traffic load can be transferred to a wider area at a relatively low cost. FIGURE 7 shows the different pavement structural layers (surface course, CCPR, aggregate, and subgrade), the placement of the three pressure plates (P1, P2, and P3) and the transfer slopes for each layer. To avoid interrupting the consolidation process, the pressure measurements at 40 kN (9 kips) wheel load after 100,000 ESALs were averaged and shown in FIGURE 7 to demonstrate the load transfer slopes in the two test cells.

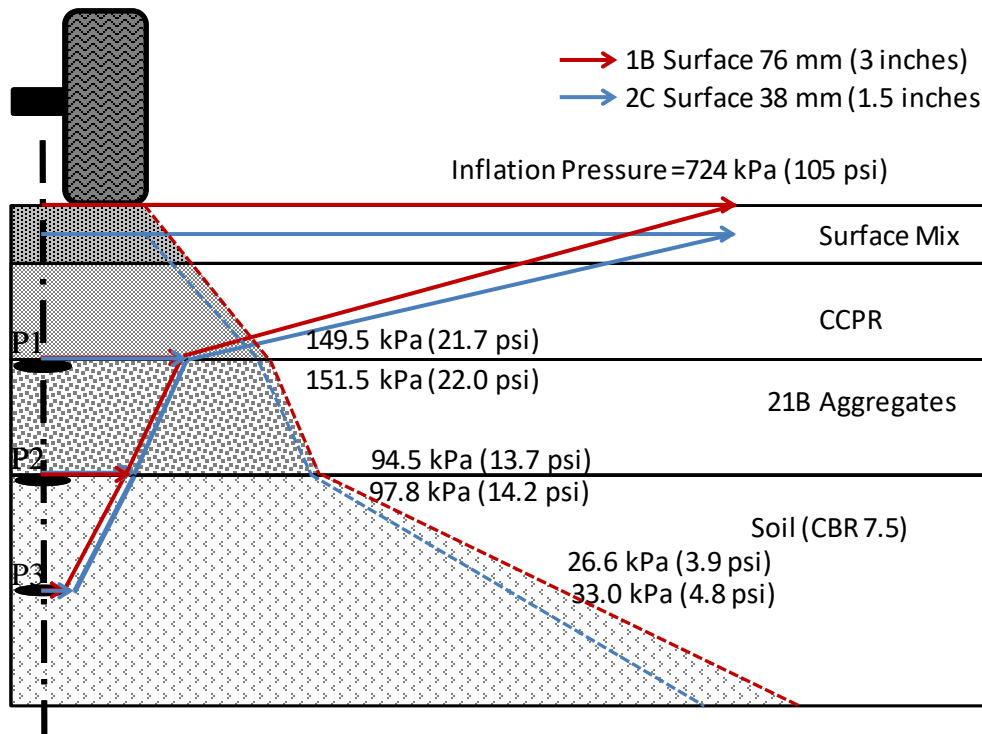


FIGURE 7 Load transferring in the pavement section.

As shown in FIGURE 7, the thinner surface layer in cell 2C leads to a bigger slope of pressure reduction in the surface and CCPR layers. From a mechanics perspective, this will induce a higher shear stress which may lead to increased rutting depths in these two layers. Similarly, the pressure in 2C's base and subgrade layers is larger than that in 1B, which might induce increased rutting as well.

Rutting Depth

The rut profiler mounted on the HVS carriage was used to scan the pavement surface for vertical permanent deformation. The difference between the daily scanned surface and the control surface scan represents the surface vertical permanent deformation (SVPD), as shown in FIGURE 4 (a). In this study, the rutting depth was calculated from SVPD measurements according to the American Association of State Highway and Transportation Officials' PP 69-14 method, as demonstrated in FIGURE 8. For each SVPD profile, rutting depth was calculated for each transverse plane, and the rutting depths of the pavement section middle part (4.88 m or 16 feet) were averaged to represent the rutting status of the test cell. The results of the four test cells are presented in FIGURE 9.

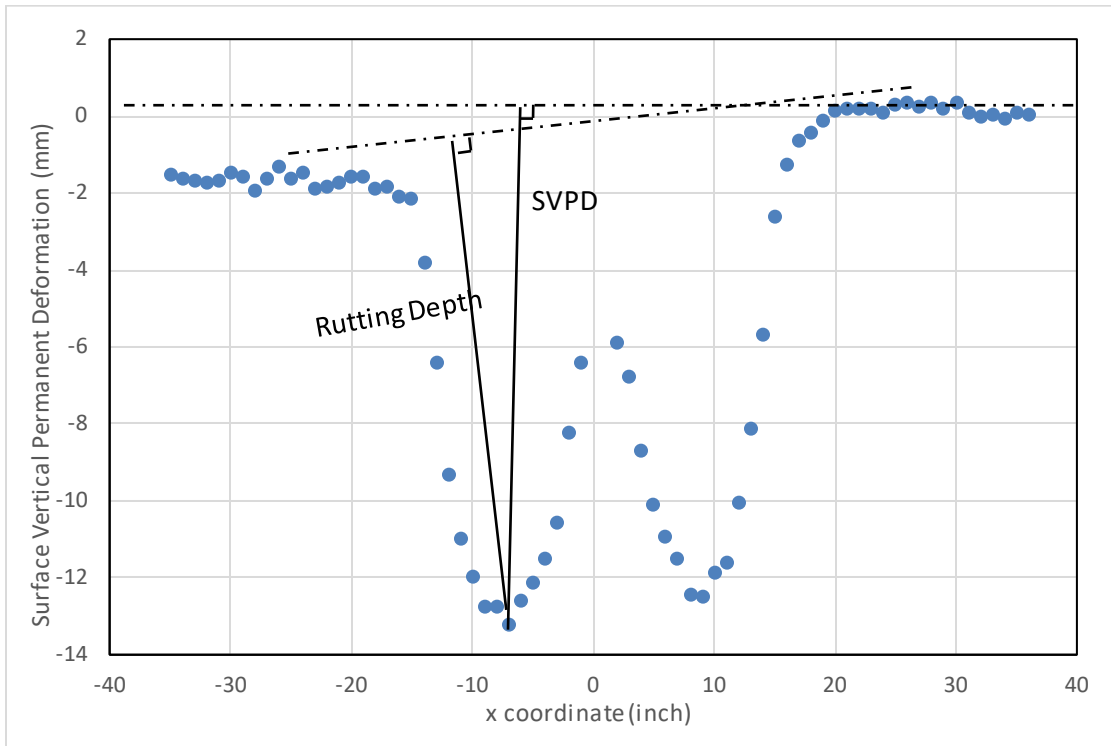


FIGURE 8 Rutting depth calculation demonstration.

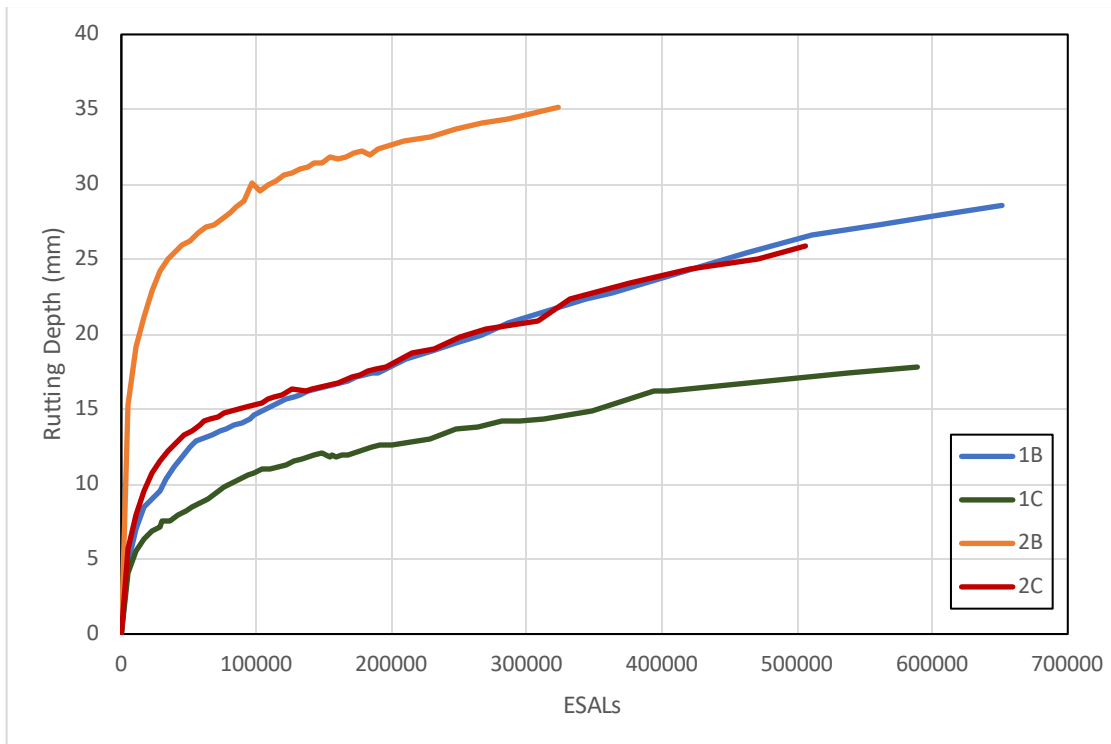


FIGURE 9 Rutting depths for the four test cells.

As shown in FIGURE 9, the shapes of the four curves were similar, but their magnitudes were quite different. Cell 2B had a much larger rutting depth than the other three cells. Specifically, the rutting depth in 2B was almost 30 mm (1.2 inches) at 10,000 ESALs; in contrast, the rutting depth in 2C was only 15 mm (0.6 inch) at 10,000 ESALs. Cells 2B and 2C consist of the same structure and materials, and were anticipated to behave similarly, but instead were found to behave quite differently.

By combining the experiment timeline in TABLE 1 with FIGURE 9, the authors found that this difference might come from the change of material properties over time. The construction of the four cells was finished on October 23, 2015. Cell 2B was the first to be tested, and it had the highest rutting depth among the four cells, and a much higher rutting depth than its twin cell, 2C. Cell 1B was tested before its twin cell 1C, and had higher rutting than 1C as well.

These observations suggest that the rutting resistance of the CCPR sections increases versus time. This finding matches well with the conclusion of Diefenderfer and Apeageyi in 2011 [7]. They found that the structural capacity of cement-based full-depth reclamation projects increased significantly by time, and the differences in the amount of strength gain depending on the stabilizing agents.

As a result, pavement age was incorporated into the rutting model as a factor, and an empirical model was developed to simulate the development of rutting depth in the four cells:

$$RD = \alpha \cdot ESAL^{\beta_1} \cdot h^{\beta_2} \cdot Age^{\beta_3}$$

where RD represents the rutting depth in mm, $ESAL$ is the number of ESALs corresponding to the rutting depth measurement, h represents the thickness of the top layer (mm), Age is the number of days passed from pavement placement to the rutting measurement, and α , β_1 , β_2 , β_3 are the coefficients to be determined by regression. This model is a log-linear model and can be written as the following equation:

$$\log(RD) = \log(\alpha) + \beta_1 \cdot \log(ESAL) + \beta_2 \cdot \log(h) + \beta_3 \cdot \log(Age) + \varepsilon$$

A linear regression was conducted based on the least square estimation method, and the fitted model of rutting depth can be expressed as:

$$RD = 24.291 \cdot ESAL^{0.342502} \cdot h^{-0.691675} \cdot Age^{0.683178}$$

The analysis of the linear regression shows that all three parameters: ESAL, thickness, and age are extremely significant (p-value < 2e-16). The fitted curves of the rutting depth in the experiment are compared with the corresponding measurements in FIGURE 10. As the figure shows, the rutting depth model explains the different rutting curves well. $R^2_{adjusted}$ is 97.56%, which means that the three parameters are all important to the rutting performance of CCPR pavement, and the combination of the three parameters explained 97.56% of the variance of rutting depth data in our experiment.

With the completed model, the rutting development in a CCPR pavement section under a known loading process can be predicted. Assuming both lane 1 and lane 2 were tested since July 25, 2016, (276 days after the placement), and the loading pace was 5,000 ESALs per day, the rutting depth developments for the pavement structures in these two lanes are illustrated in FIGURE 11.

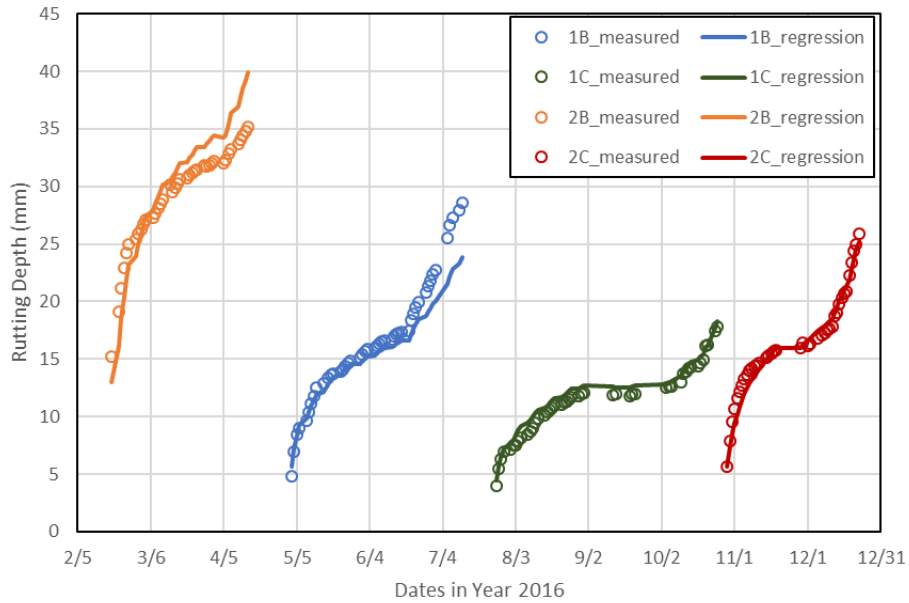


FIGURE 10 Comparison among the regression fitted results with rutting depth measurements.

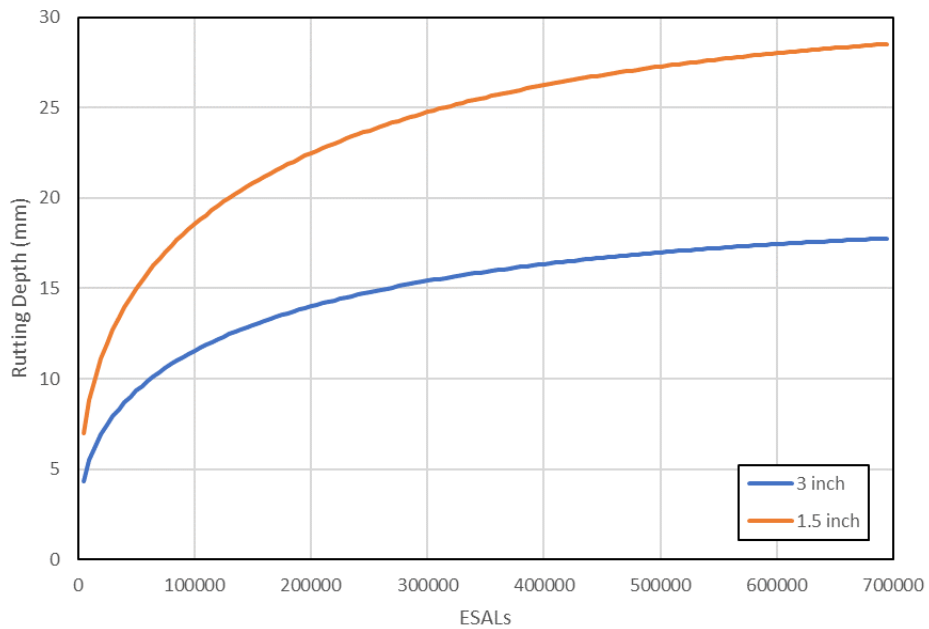


FIGURE 11 Rutting depth predictions for 3-inch and 1.5-inch pavement sections.

As shown in FIGURE 11, the developed model predicts that the rutting depth in a 76-mm (3-inch) -surface-layer structure increases much more slowly than in a 1.5-inch-surface-layer structure. If measured at 700,000 ESALs, the 76-mm (3-inch) structure has a rutting depth of 17.8 mm (0.7 inch), about 62.2% of the 38-mm (1.5-inch) structure’s rutting depth of 28.5 mm (1.1 inch).

DISCUSSION

Only the strain at the bottom of CCPR layer was monitored during the experiment. The strain in lane 2 (38-mm [1.5-inch] surface layer) was similar to that in lane 1 (76-mm [3-inch] surface layer) at the beginning, but grew larger than lane 1 after 300,000 ESALs.

The pressure decreased as the depth increased as expected prior to the experiment. The difference in the magnitude of pressure between the two lanes was clear above and in the middle of the subgrade, but was less discernable at the bottom of the CCPR layer. One possible reason is that the thinner surface layer induced a higher shear stress within the structure and affected the sub-base layers as a result. Another possible reason is that the water table within the sub-base layers may have been different during the tests, which may have affected the pressure distribution.

The analysis of the load transferring process suggests that wheel load was distributed in a smaller area within the sub-layers of the 38-mm (1.5-inch)-surface-layer structure. This induced a more concentrated pressure distribution and a higher shear stress within the entire structure, eventually resulting in larger rutting depth distributions as reflected on the pavement's surface.

The rutting depths within the four test cells were quite different because the rutting resistance of the CCPR section increased over time after initial placement. The gained strength probably came from the curing effect of Portland cement, which was added to the formed bitumen as the stabilizing agent. The test cells were placed at the same time, but tested at different times during a one year period, making their material properties different during testing, and inducing significant difference in rutting depth.

To quantify the variance brought in by the time component, a model of rutting depth was developed with the age of pavement sections by days incorporated as a factor. The model fitted the measurements well, with a R^2_{adjusted} equal to 97.56%. The effect of pavement age by days was recognized as significant with a p-value smaller than 2×10^{-16} . As this result shows, incorporating the age of pavement sections in the analysis of pavement rutting depth could explain the variance between pavement sections with the same structure and loading history that are tested at different ages.

CONCLUSIONS

The following conclusions can be drawn from the results:

- The water table within the sub-base layers may affect the distribution of pressure and pressure cell reading as a result.
- The use of the thinner surface layer over CCPR base layer resulted in a steeper slope of pressure reduction and thus higher vertical stresses throughout the pavement.
- The rutting resistance of the CCPR pavement in this study increased over time, and the model of rutting performance could be improved by adding pavement age as a factor.
- The pavement section with the 76-mm (3-inch) HMA surface layer developed approximately 62% of the rutting depth of the section with the 38-mm (1.5-inch) surface layer.

REFERENCES

1. Liu, X., Q. Cui, and C. Schwartz, *Performance Benchmark of Greenhouse Gas Emissions from Asphalt Pavement in the United States*, in *ICSI 2014: Creating Infrastructure for a Sustainable World*. 2014. p. 678-689.
2. Stroup-Gardiner, M., National Academies of Sciences, Engineering, and Medicine, *NCHRP Synthesis 421: Recycling and Reclamation of Asphalt Pavements Using In-Place Methods*. The National Academies Press, 2011.
3. Thompson, M.R., L. Garcia, and S.H. Carpenter, *Cold In-place recycling and full depth recycling with asphalt products (CIR&FDRwAP)*. 2009, Illinois Center for Transportation (ICT).
4. Apeageyi, A.K. and B.K. Diefenderfer, *Evaluation of cold in-place and cold central-plant recycling methods using laboratory testing of field-cored specimens*. *Journal of Materials in Civil Engineering*, 2012. **25**(11): p. 1712-1720.
5. Diefenderfer, B.K., et al., *Dynamic Modulus of Recycled Pavement Mixtures*. *Transportation Research Record: Journal of the Transportation Research Board*, 2016(2575): p. 19-26.
6. Timm, D.H., M.D. Sánchez, and B.K. Diefenderfer. *Field Performance and Structural Characterization of Full-Scale Cold Central Plant Recycled Pavements*. in *Transportation Research Board 94th Annual Meeting*. 2015.
7. Diefenderfer, B. and A. Apeageyi, *Time-dependent structural response of full-depth reclamation*. *Transportation Research Record: Journal of the Transportation Research Board*, 2011(2253): p. 3-9.